



## EPR dosimetry of yttria micro rods

S.C. Santos\*, O. Rodrigues Jr., L.L. Campos

Instituto de Pesquisas Energeticas e Nucleares – IPEN, Av. Prof. Lineu Prestes 2242, Cidade Universitaria, São Paulo, Brazil



### ARTICLE INFO

#### Article history:

Received 16 November 2017

Received in revised form

22 January 2018

Accepted 24 January 2018

Available online 31 January 2018

#### Keywords:

Yttria

Rare earths

Lanthanides

EPR

Radiation dosimetry

Ceramic processing

### ABSTRACT

The use of rare earths (RE) as dopant of materials has led the development of advanced materials for many applications such as optical tracers, special alloys, semiconductors, as well as radiation dosimeters. The development of new dosimetric materials based on REs is a great challenge in innovation of materials. Yttria ( $\text{Y}_2\text{O}_3$ ) presents luminescent properties and is a promising material for radiation dosimetry. The present paper aims to evaluate paramagnetic defects of  $\text{Y}_2\text{O}_3$  rods obtained via bio-prototyping by using Electron Paramagnetic Resonance (EPR) technique at room temperature. Ceramic rods were irradiated with gamma doses from 0.001 to 150 kGy and evaluated by EPR at room temperature with X-band EPR. According to EPR results, as sintered samples exhibited an EPR signal with principal g tensor of 2.020 and maximum line width around 2.3 mT, which is ascribed to interstitial oxygen ion. Dose response behaviour exhibited two distinct dose ranges, one is from 1 to 100 Gy and the second is from 0.1 to 70 kGy. Thermal annealing approaches reveal that defect centres of yttria decay significantly at high temperature. These innovative results make  $\text{Y}_2\text{O}_3$  a promising material for radiation dosimetry.

© 2018 Elsevier B.V. All rights reserved.

### 1. Introduction

Electron Paramagnetic Resonance (EPR) is a powerful, versatile, non-destructive and nonintrusive characterization technique, which yields meaningful structural and dynamical information from chemical and physical processes. EPR applications include polymerization reactions [1], spin trapping [2], catalysis [3], defects in crystals i.e. colour centres [4], laser [5], radiation effects and damage [6], free radicals in living tissues and fluids [7], drug detection [8], hybrid supercapacitors [9], semiconductors [10]. Therefore, EPR is a powerful tool for solid state dosimetry.

Rare earth elements (RE) present unique chemical and physical properties, which are very useful for applications as semiconductors, luminescent devices, capacitors, special alloys and also in radiation dosimetry [11–15]. Dysprosium doped calcium sulphate ( $\text{CaSO}_4:\text{Dy}$ ) is used as thermoluminescent dosimeter, which is applied for beta [16], gamma [17], X [18], electrons [19], photons [20], UV [21] and laser dosimetry [22].  $\text{CaSO}_4:\text{Dy}$  dosimeter exhibits excellent reproducibility, high sensitivity (40 times higher than  $\text{LiF}: \text{Mg,Ti}$ ) [23], AO [24] and RPE [25] properties.

The development of new dosimetric materials with luminescent and paramagnetic response higher than commercial dosimeters is a

challenge in innovation of materials. Among RE, yttria ( $\text{Y}_2\text{O}_3$ ) is a promising material for radiation dosimetry due to unique properties as melting point of 2400 °C, refractive index of 1.9, specific heat capacity of  $0.45 \text{ J g}^{-1} \text{ K}^{-1}$ , and Dielectric strength of  $11 \text{ kV mm}^{-1}$  [26]. Besides,  $\text{Y}_2\text{O}_3$  is used for improving characteristics of many advanced materials such as, sintering [27], catalysis [28], luminescence [29], electrical [30], electronic [31], mechanical [32] and thermal [33]. Yar et al. [34] synthesized highly uniform nano-sized yttrium doped tungsten oxide particles ( $\text{WO}_3:\text{Y}_2\text{O}_3$ ) by chemical reaction. Samples sintered at 1400 °C showed higher relative density ( $R_D$  of 95%) and finer grain size as compared to ones sintered at 1500 °C and 1600 °C. Li et al. [35] produced yttrium doped zinc oxide nanofibers ( $\text{ZnO:Y}_2\text{O}_3$ ) by electrospinning method followed by calcination. As a result, doping with yttrium was useful to form particles with uniform morphology, higher specific surface area ( $40.2 \text{ m}^2 \text{ g}^{-1}$ ) and gas sensing as compared to ones ZnO. Europium doped yttria ( $\text{Y}_2\text{O}_3:\text{Eu}^{3+}$ ) is noted for its excellence in luminescence [36]. ZHANG et al. [37] reported the synthesis of single-layer yttria nanosheets doped with  $\text{Eu}^{3+}$  and  $\text{Tb}^{3+}$  by the exfoliation method. The promising results such as transparency, strong red and green emissions show that nano sheets have potential to be used as building blocks and other functional materials.

Based on  $\text{Y}_2\text{O}_3$  potentiality, the present work reports an EPR characterization of yttria rods formed by colloidal processing as an approach to evaluate this promising rare earth at room temperature for radiation dosimetry.

\* Corresponding author.

E-mail address: [silas.cardoso@alumni.usp.br](mailto:silas.cardoso@alumni.usp.br) (S.C. Santos).

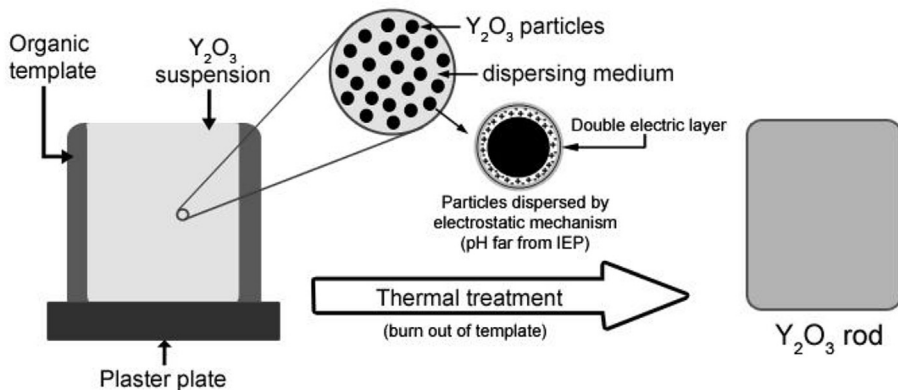


**Fig. 1.** Formation of yttria rods by bio-prototyping.

**Table 1**

Processing parameters to form yttria micro rods by bio-prototyping.

Particle characteristics	$d_{50}$ (nm)	$d_c$ (nm)	$\rho$ ( $\text{g} \cdot \text{cm}^{-3}$ )	$C_s$
	410.0	4.42	4.94	Cubic type-C
Suspension	Solids (%vol)	pH	$\eta$ (mPa.s)	Binder (wt.%)
	20.0	10.0	210.0	0.40
Sintering	$H_R$ ( $^{\circ}\text{C} \cdot \text{min}^{-1}$ )	Temp ( $^{\circ}\text{C}$ )	Slope (h)	Atmosphere
	5	1600	4	Air

$d_{50}$ : mean particle size;  $d_c$ : crystallite size;  $\rho$ : pycnometric density;  $C_s$ : crystalline structure;  $\eta$ : apparent viscosity at  $10\text{s}^{-1}$ ;  $H_R$ : heating rate; Temp: temperature.

## 2. Experimental

Yttria rods were produced by bio-prototyping according our recent study [38] as illustrated in Fig. 1. The morphology and size evaluation of yttria rods were performed by optical microscopy (OM, Nikon SMZ1270). Besides, microstructure formation was observed by scanning electron microscopy (SEM, Oxford Instruments).

Batches of four yttria rods were irradiated with gamma source with dose range from 0.001–100 kGy in electronic equilibrium conditions and room temperature ( $20^{\circ}\text{C}$ ). Crystal defects and radicals induced by ionizing radiation were characterized by electron paramagnetic resonance at room temperature ( $20^{\circ}\text{C}$ ) and room atmosphere (air) using X-band EPR spectrometer (Bruker EMX PLUS).

EPR spectra of samples were recorded using the following

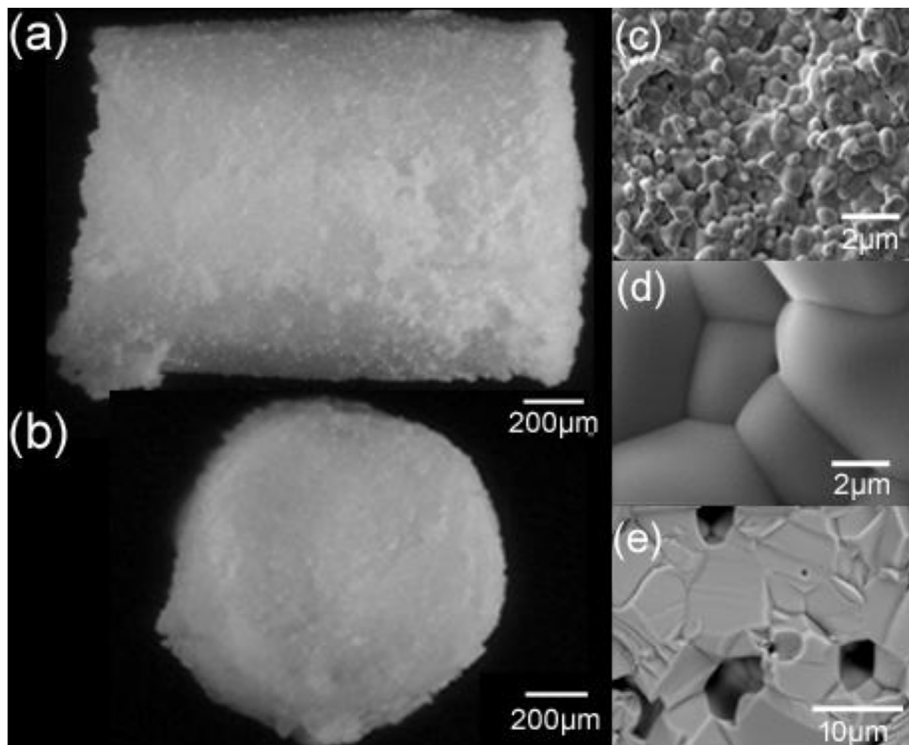


**Fig. 2.** Yttria micro rod produced by bio-prototyping: OM images of rod in (a) side view; (b) top view; SEM images of microstructure of (c) external surface; (d) zoom in on external surface exhibiting grains with size higher than  $2\text{ }\mu\text{m}$ ; and (e) inner surface showing cleavage planes characteristic of fragile fracture.

parameters: field frequency modulation of 100 kHz, microwave power of 0.6325 mW, centre field at 320 mT, sweep width of 600 mT, modulation amplitude of 4 G, time constant of 0.01 ms and, 10 scans. The EPR response of irradiated samples was determined as a mean of each batch normalized by mean mass of containing samples. EPR dose response and time decay curves were plotted considering the mean of peak-peak amplitudes of irradiated samples.

### 3. Results and discussion

Nowadays, dosimetric materials are inorganic crystalline materials nominally addressed as phosphors ascribe to their characteristic luminescence as suitably excited. These materials are usually in the form of discs, square chips, rods, films, pellets, single crystals or nano/micro powders. For this work, micro rods of yttria were produced by bio-prototyping. Table 1 lists processing

parameters for bio-prototyping of ceramic samples according to our recent work [38].

As can be seen, yttria micro rods exhibit rough surface, diameter and height of 3.335 x 2,271 mm, respectively (Fig. 2a and Fig. 2b). Besides, the control of stability of particles in suspension enables the conformation of ceramic samples by many shaping process such as casting, tape casting, extrusion, dip coating, bio-prototyping. Furthermore, stable suspensions lead to formation of higher packing of particles, avoiding voids during shaping and drying. As a consequence, samples with suitable mechanical strength and dense microstructure are usually formed after sintering as shown in Fig. 2d. As fractured rods exhibited dense-homogeneous microstructure, containing grains which size is higher than 1 μm.

Crystalline structure of yttria rods was confirmed by XRD curves as shown in Fig. 3a. All XRD peaks coincided to PDF 70-603, which describes that  $\text{Y}_2\text{O}_3$  has cubic C-type type (Fig. 3b) [39], Ia3 space

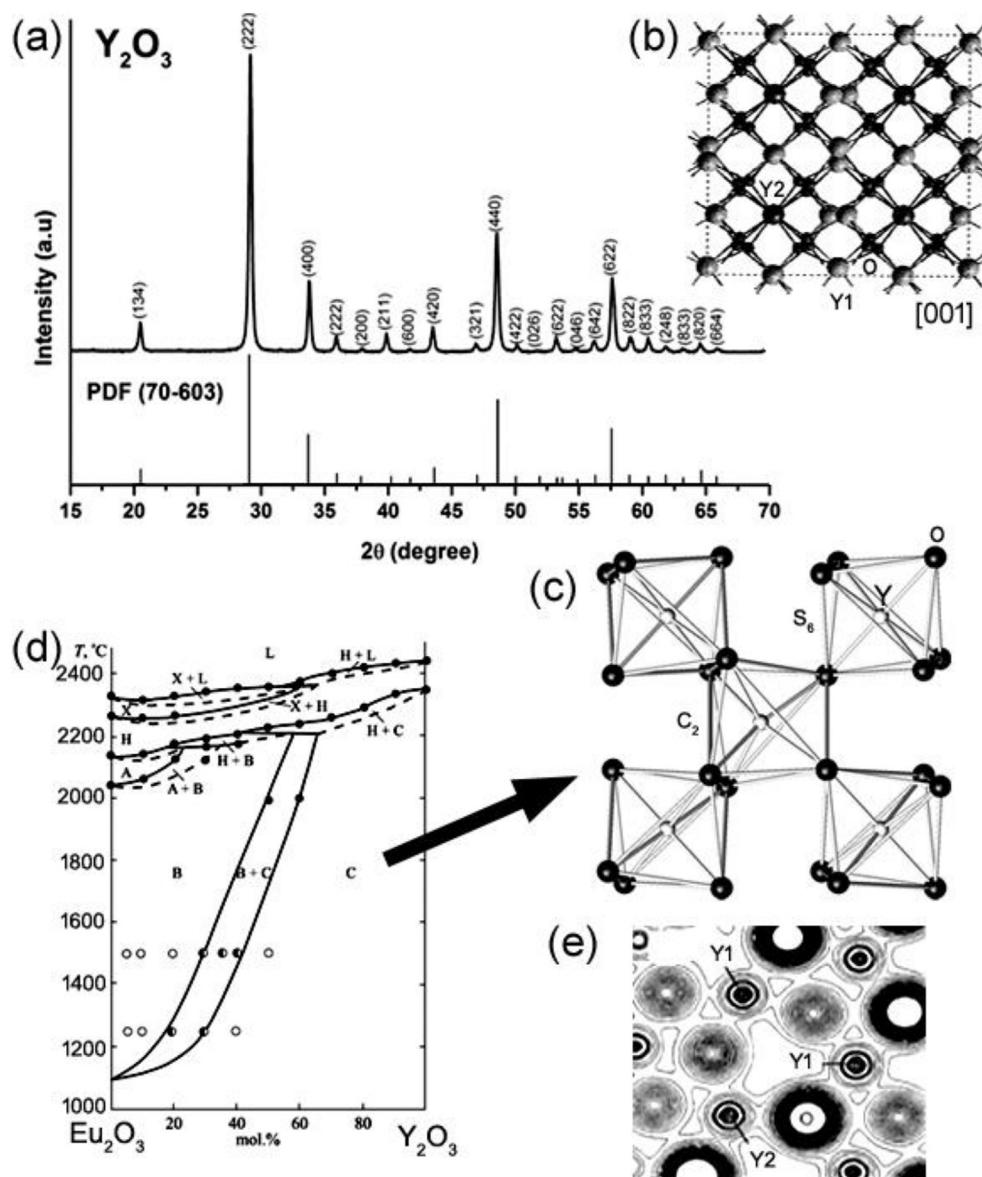


**Fig. 3.** Crystal characterization of yttria rods: (a) XRD curves of  $\text{Y}_2\text{O}_3$  cubic C-type; (b) crystal lattice along [001] direction; (c) cation sites  $\text{C}_2$  and  $\text{S}_6$  in cubic C-type structure; (d) phase equilibria diagram of  $\text{Y}_2\text{O}_3$ - $\text{Eu}_2\text{O}_3$  system exhibiting all field of composition of yttria, in which cubic C-type is the most predominant structure; (e) valence charge diagram in a plane exhibiting  $\text{Y}_1$ - $\text{O}$ - $\text{Y}_2$  bonding and void spaces.

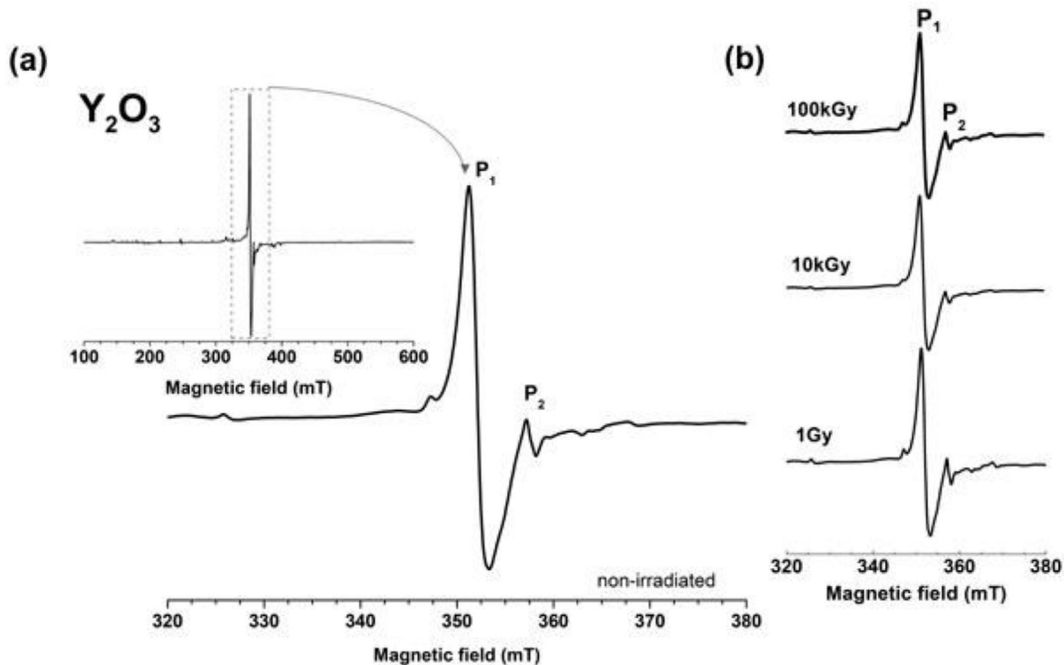


**Fig. 4.** EPR spectra recorded at room temperature and atmosphere for  $\text{Y}_2\text{O}_3$  rods irradiated with doses from 0 to 100 kGy.

group, sixteen formula units per unit cell, coordination number (N) of 6 and two points symmetry  $S_6$ ,  $C_3$  and  $C_2$  (Fig. 3c) [40]. Among 32 ions, 24 ions occupy sites with  $C_2$  symmetry, whereas 8 ions occupy  $S_6$ . The local axes of the  $S_6$  sites are in the  $[111]$ ,  $[\bar{1}11]$ ,  $[1\bar{1}\bar{1}]$ , and  $[1\bar{1}\bar{1}]$  directions. The  $C_2$  axes are parallel to  $[100]$ ,  $[010]$ , or  $[001]$ . The  $S_6$  site has small crystal field and inversion centre, in which electron-dipole transitions are not allowed. However, thermal fluctuations of crystal lattice destroy the  $S_6$  symmetry locally,

which provides the possibility of electron-dipole transition occur [41]. In addition,  $C_2$  symmetry has no centre of inversion, which enables electron-dipole transitions and consequently luminescent emissions as doped with RE ions.

All sesquioxides as  $\text{Dy}_2\text{O}_3$ ,  $\text{Th}_2\text{O}_3$ ,  $\text{Ga}_2\text{O}_3$  and  $\text{Ln}_2\text{O}_3$  exhibit C-type structure [42]. Nevertheless, monoclinic [43], fluorite and hexagonal [44,45] structures were also reported for yttria. Based on phase equilibria diagram of  $\text{Eu}_2\text{O}_3 - \text{Y}_2\text{O}_3$  system (Fig. 3d) [46] yttria exhibits large range of compatibility in which cubic C-type is

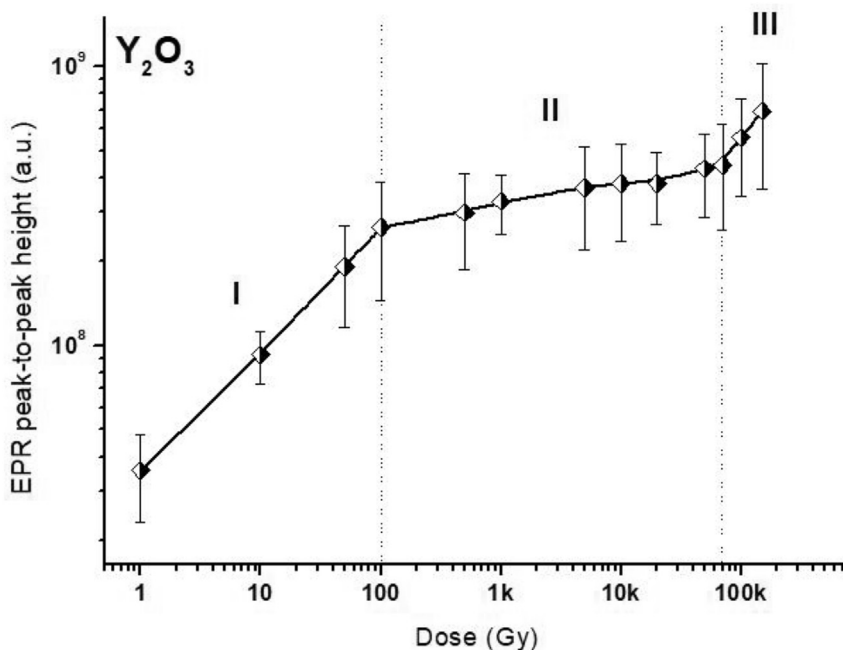


**Fig. 5.** EPR dose response of  $\text{Y}_2\text{O}_3$  rods as a function of absorbed irradiation dose from 0.001 up to 150 kGy at ambient temperature and atmosphere.

formed. This range increases as a function of yttria content e.g. 10 mol.%  $\text{Y}_2\text{O}_3$  provides C-type phase stability up to 1100 °C, whereas 100 mol.% up to 2300 °C.

Some investigations reported that the nature of bonding between Y-O is not completely ionic [47]. Nian Xu et al. [39] reported a theoretical study on the bond order of  $\text{Y}_2\text{O}_3$ , which means a quantitative measure of the strength of the bond for Y and O in crystal lattice of  $\text{Y}_2\text{O}_3$  (Fig. 3e) [39]. From this study, the chemical bond of  $\text{Y}_2\text{O}_3$  is far from fully ionic and the bonding between Y and O is significantly covalent. Using valence charge density maps authors reported that the cubic structure of  $\text{Y}_2\text{O}_3$  is less closed packed, exhibiting large vacancies for Y and O planes. These vacancies enable RE ions incorporation and formulation of luminescent yttria-based materials ( $\text{Y}_2\text{O}_3:\text{RE}$ ).

EPR spectrum of unirradiated  $\text{Y}_2\text{O}_3$  rods at room atmosphere

and temperature is shown in Fig. 4a. As can be see, ceramic rods exhibited EPR a signal  $P_1$  with principal g tensor of 2.020 and line width around 2.3 mT, and a lower intensity signal  $P_2$  with principal g tensor of 2.040 and line width around 2.3 mT. Irradiation of samples with dose range up to 100 kGy created no new defect centres, as illustrated in Fig. 5b. Indeed, it led to increase of the main EPR signal ( $P_1$ ), which means that more trapped electrons at anionic vacancies were produced. In addition, two very low intensity signals on the left side of spectra with g tensor values of 2.1604 and 2.0296 respectively, and may be ascribed to impurities of yttria. Considering that rare earths are found in nature with others rare earths and their extraction, which means their purification is a process extremely complex, the presence of impurities even in very low concentration can be observed. The investigation of these two very small signals is beyond the aim of the present study.

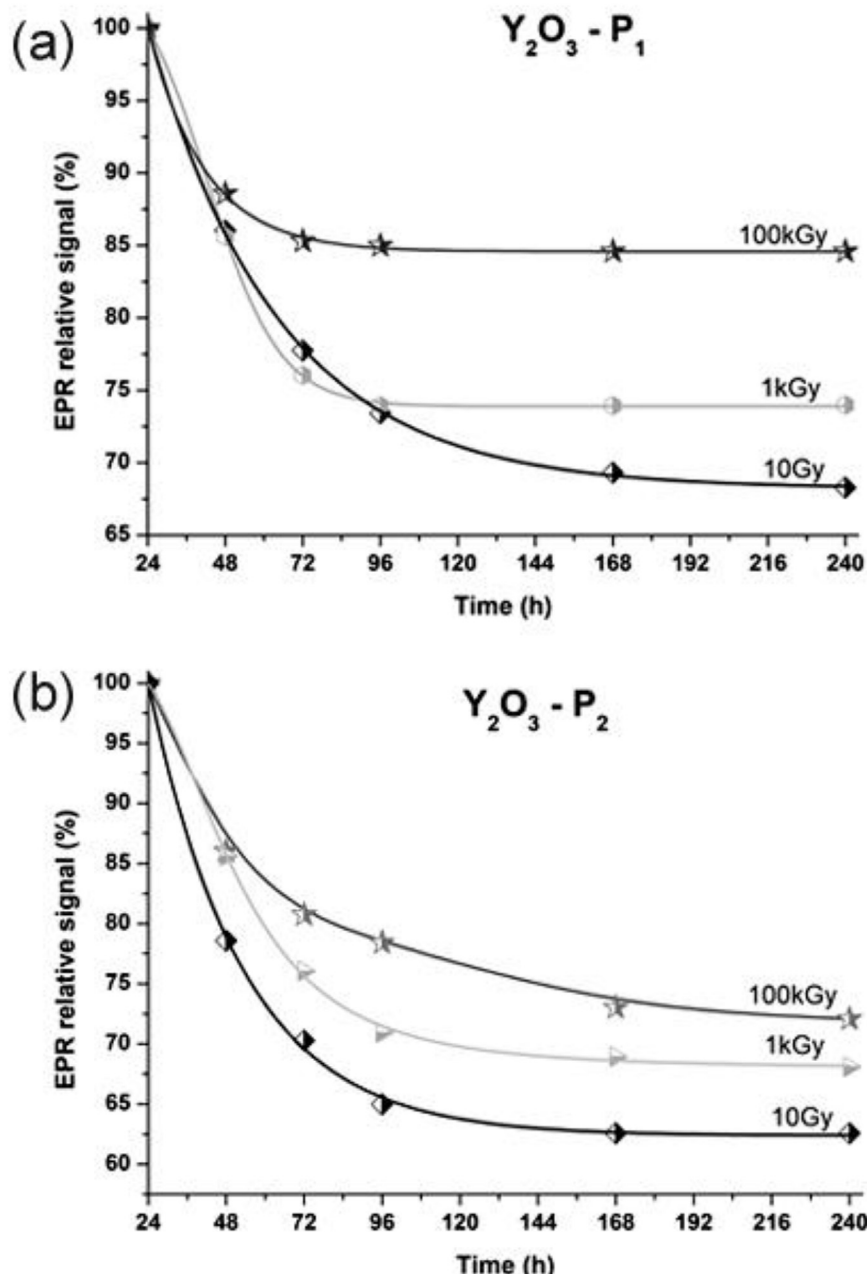


Fig. 6. EPR signal fading of centres (a)  $P_1$  and (b)  $P_2$  of  $\text{Y}_2\text{O}_3$  rods evaluated at room temperature during 240 h.

The observed defect addressed as  $P_1$  is ascribed to interstitial  $O^{2-}$  ion, nominally addressed as superoxide ion, which is generated by adsorption of molecular oxygen as observed by Lunsford [48]. In addition, oxygen can be either removed from the bulk of material with subsequent diffusion to surface or from surface by means of electron irradiation, annealing, sputtering, exposure to x-rays, or chemical reaction [49–54]. Osada et al. [55] reported that 10 mol%  $Y_2O_3$ -CaO powders annealed at oxygen atmosphere exhibited g values of 2.070 and 2.040, respectively. On the other hand, none of these signals was observed at vacuum. Singh et al. [56] observed for  $Y_2O_3$ :Er, in which the main signal was nominally addressed as centre I, exhibiting as characteristic g values of 2.0415 and 2.0056, respectively. In addition, it was reported that even though centre I signal was intense, it presented significant decay at low temperature around 160 °C.

Upon no irradiated sample (Fig. 4a), the low intensity centre ( $P_2$ ) exhibited line width around of 13G and g tensor of 1.969. This centre is assigned to  $F^+$  centre charged vacancy oxygen having one remaining electron. Besides, C-type crystal lattice of  $Y_2O_3$  presents intrinsic oxygen vacancies that can produce F centres close to  $P_2$ . For irradiated samples no significant change in  $c_2$  shape and intensity was observed.

The effect of the  $P_2$  on luminescence of  $Y_2O_3$  thins was discussed previously by Bourdun [57]. Thermal treatment of  $Y_2O_3$  samples in air atmosphere leads to the filling the oxygen vacancies by oxygen atoms from air into  $Y_2O_3$  and as a result, additional weak bonds with oxygen ions are formed. On irradiation a radiative recombination between these new centres and those intrinsic centres occurs, resulting in an increase of the luminescence near 2.9 eV. Costantini et al. [58] reported the characteristic centre  $P_2$  with principal g values of 1.966 and 1.972 as investigating yttria stabilized zirconia (YSZ). Singh et al. [56] evaluated the stability of  $c_2$  as a function of temperature and observed that this centre decays at low temperature around 180 °C.

The dose dependence of any material is the fundamental basis of its application as a dosimetric material. Within the dose range of interest defined the response is expected to be reproducible as a function of dose and preferably linear. Linearity describes

proportionality between EPR signal and absorbed dose. Usually, the dose response behaviour of most dosimetric materials exhibits linear, supralinear and saturating response.

In this work, the EPR signal as a function of gamma radiation absorbed dose, determinated as peak height of the main centre ( $P_1$ ), exhibited two distinct dose response behaviours (Fig. 5). The first linear range (I) with expressive EPR peak-to-peak increase was from 1 to 100 Gy, which means the sensitiveness of yttria for low doses. The second range (II) from 0.1 to 70 kGy exhibited small increase of EPR peak-to-peak, which reveals that higher doses were not effective to provide significant defects in yttria. A new slope is formed apart from 70 kGy which might correspond to formation of new defects and a third range. Considering that a dose of 150 kGy is extremely high for dosimetry application, higher doses were not evaluated in this work.

Fading of  $Y_2O_3$  rods irradiated with doses up to 150 kGy at room temperature was evaluated considering EPR relative signal during eleven days (Fig. 6). It is observed that the centre  $P_1$  (Fig. 6a) decays relatively moderated, wherein samples irradiated with 10 Gy exhibited fading of 32% and samples irradiated with 1 and 100 kGy presented lower fading around of 25 and 15%, respectively. Apart from 168 h (seven days)  $P_1$  maintained at least 70% of its original signal. On the other hand, it is seen that centre  $P_2$  (Fig. 6b) which is ascribed to new centres formed during irradiation, exhibited fading behaviour like centre  $P_1$ . Even though oxygen from air form weak bond into  $Y_2O_3$ , the new electronic defects are quite stable over 240 h with fading around of 37%

The stability of centres  $P_1$  and  $P_2$  were measured by means of annealing approach up to 1200 °C and at environmental atmosphere. The thermal annealing behaviour of centre  $P_1$  is illustrated in Fig. 7a. According to results,  $P_1$  EPR relative response decays significantly at high temperature ( $T > 600$  °C). Singh et al. [56] reported low temperature decay around of 160 °C for  $Y_2O_3$ :Er samples irradiated with 5 kGy. In addition, centre  $P_2$  (Fig. 7b) exhibited similar annealing behaviour. Considering that yttria lattice exhibits a large number of vacancies, one of the most probable defects is  $F^+$  centre, which means an electron trapped at an anion vacancy. Such defect were observed by Singh [56] and Hutchison [59].

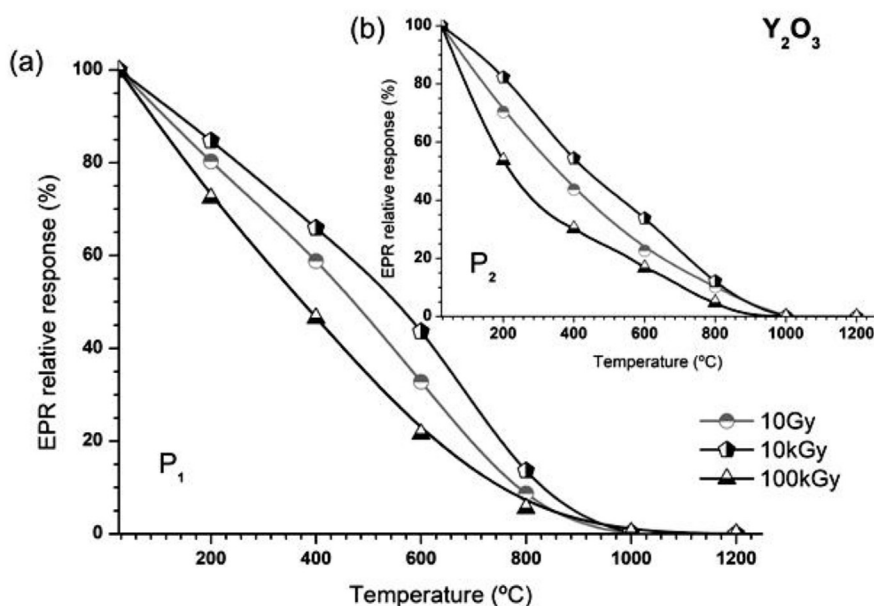


Fig. 7. Thermal annealing behaviour of centres (a)  $P_1$  and (b)  $P_2$  of  $Y_2O_3$  rods.

## 4. Conclusion

Yttria rods with dense microstructure were produced by bio-prototyping and followed by sintering at 1600 °C for 4 h at room atmosphere. Ceramic samples exhibited an EPR signal with principal g tensor of 2.020 and maximum line width around 2.3 mT is ascribed to interstitial oxygen ion. Dose response behaviour exhibited two distinct dose ranges, one is from 1 to 100 Gy and the second is from 0.1 to 70 kGy. Irradiated samples exhibited fading stability from 96 h. Thermal annealing approaches reveal that defect centres of yttria decay significantly at high temperature. According to results, yttria is a promising material to be used for radiation dosimetry.

## Acknowledgements

We authors are deeply grateful to MSc. Douglas Will Leite and MSc. William Naville from The University Center of FEI, grant #2014/23621-3 from São Paulo Research Foundation (FAPESP) São Paulo Research Foundation; National Council for Scientific and Technological Development; and Coordination for Improvement of High Degree People (CAPES).

## References

- [1] F.F. Li, L.Q. Xiao, L.J. Liu, Polymeric palladium-mediated carbene polymerization, *Polym Chem-Uk* 6 (2015) 6163–6170.
- [2] C.J. Rhodes, The role of ESR spectroscopy in advancing catalytic science: some recent developments, *Prog. React. Kinet. Mech.* 40 (2015) 201–248.
- [3] R.R. Cheng, Z.L. Wu, Y.L. Hou, J. Dong, J.Z. Cui, B. Zhao, Three Cu(II) coordination polymers with novel bi-triazole ligand: synthesis, structure and EPR properties, *Inorg. Chem. Commun.* 51 (2015) 95–98.
- [4] N.F. Cano, L.H.E. dos Santos, J.F.D. Chubaci, S. Watanabe, Study of luminescence, color and paramagnetic centers properties of albite, *Spectrochim. Acta A* 137 (2015) 471–476.
- [5] N.E. Domracheva, V.E. Vorobeva, M.S. Gruzdev, A.V. Pyataev, Blue shift in optical absorption, magnetism and light-induced superparamagnetism in gamma-Fe2O3 nanoparticles formed in dendrimer, *J. Nanoparticle Res.* 17 (2015).
- [6] V.V. Halyan, A.A. Konchits, B.D. Shanina, S.V. Krasnovyd, O.O. Lebed, A.H. Kevshyn, M.V. Shevchuk, A.V. Bodnaruk, V.O. Yukhymchuk, EPR of gamma-induced defects and their effects on the photoluminescence in the glasses of the Ag0.05Ga0.05Ge0.95S2-Er2S3 system, *Radiat. Phys. Chem.* 115 (2015) 189–195.
- [7] M. Hashem, M. Weiler-Sagie, P. Kuppusamy, G. Neufeld, M. Neeman, A. Blank, Electron spin resonance microscopic imaging of oxygen concentration in cancer spheroids, *J. Magn. Reson.* 256 (2015) 77–85.
- [8] M.A. Morisy, A.N.M. Kawde, Electron paramagnetic resonance monitoring for on-demand electrochemically-generated radicals, *Electrochim. Acta* 160 (2015) 22–27.
- [9] R. Genc, M.O. Alas, E. Harputlu, S. Repp, N. Kremer, M. Castellano, S.G. Colak, K. Ocakoglu, E. Erdem, High-capacitance hybrid supercapacitor based on multi-colored fluorescent carbon-dots, *Sci Rep-Uk* 7 (2017) 11222.
- [10] H. Kaffelen, K. Ocakoglu, R. Thomann, S. Tu, S. Weber, E. Erdem, EPR and photoluminescence spectroscopy studies on the defect structure of ZnO nanocrystals, *Phys. Rev. B* 86 (2012), 014113.
- [11] A. Golev, M. Scott, P.D. Erskine, S.H. Ali, G.R. Ballantyne, Rare earths supply chains: current status, constraints and opportunities, *Resour. Pol.* 41 (2014) 52–59.
- [12] S. Massari, M. Ruberti, Rare earth elements as critical raw materials: focus on international markets and future strategies, *Resour. Pol.* 38 (2013) 36–43.
- [13] U.S.G.S. U.S. Geological Survey, Mineral commodity Summaries 2014, in, Virginia, 2014, pp. 196.
- [14] C. Centro de Gestão e Estudos Estratégicos, Uso e aplicações das Terras Raras no Brasil 2012–2030, in, Centro de Gestão e Estudos Estratégicos (CGEE), 978-85-60755-64-6, 2013, pp. 254.
- [15] C. Zhanheng, Global rare earth resources and scenarios of future rare earth industry, *J. Rare Earths* 29 (2011) 1–6.
- [16] T.N.O. Pinto, P.L. Antonio, L.V.E. Caldas, Measuring TL and OSL of beta radioisotopes inside a glove box at a radiopharmacy laboratory, *Radiat. Meas.* 46 (2011) 1847–1850.
- [17] N. Shinde, N.S. Dhoble, S.C. Gedam, S.J. Dhoble, Thermoluminescence characteristics of Na-3 SO4 Cl:X (X=Ce, Dy, Mn) phosphor, *Radiat. Eff. Defect Solid* 169 (2014) 361–367.
- [18] E.L. Correia, J.O. Silva, V. Vivolo, M.P.A. Potiens, K.A.C. Daros, R.B. Medeiros, Intensity variation study of the radiation field in a mammographic system using thermoluminescent dosimeters TLD-900 (CaSO4:DY), *Radiat. Phys. Chem.* 95 (2014) 116–118.
- [19] J.R. Cortes, R.A. Romero, J.A. Nieto, T.R. Montalvo, Electron absorbed dose measurements in LINACs by thermoluminescent dosimeters, *Appl. Radiat. Isot.* 83 (2014) 210–213.
- [20] S. Chatterjee, A.K. Bakshi, R.A. Kinikar, G. Chourasiya, R.K. Kher, Response of CaSO4:Dy phosphor based TLD badge system to high energy electron beams from medical linear accelerator and estimation of whole body dose and skin dose, *Radiat. Meas.* 44 (2009) 257–262.
- [21] J. Roman, T. Rivera, I.B. Lozano, R. Sosa, G. Alarcon, Luminescent characteristics of CaSO4:Dy films obtained by spray pyrolysis method, *Appl. Radiat. Isot.* 70 (2012) 1403–1406.
- [22] S. Chaurasia, M. Kumar, A.K. Poswal, D.S. Munda, L.J. Dhareshwar, R.K. Kher, G. Chourasiya, Comparison of thermo-luminescent detectors and X-ray vacuum detectors for measurement of X-ray yield from gold plasma produced by a sub-nanosecond Nd:glass laser, *Nucl. Instrum. Meth. A* 595 (2008) 395–400.
- [23] A. Piaskowska, B. Marczevska, P. Bilski, A. Mandowski, E. Mandowska, Photoluminescence measurements of LiF TL detectors, *Radiat. Meas.* 56 (2013) 209–212.
- [24] A.K. Bakshi, S.N. Jha, L. Olivi, D.M. Phase, R.K. Kher, D. Bhattacharyya, X-ray absorption spectroscopy and X-ray photoelectron spectroscopy studies of CaSO4 : Dy thermoluminescent phosphors, *Nucl. Instrum. Meth. B* 264 (2007) 109–116.
- [25] B. Sanyal, V. Natarajan, S.P. Chawla, A. Sharma, TL and EPR studies of CaSO4: Dy phosphor to investigate its efficacy in measurement of food irradiation dose at sub-ambient temperatures, *Radiat. Meas.* 45 (2010) 899–905.
- [26] S.C. Santos, O.J. Rodrigues, L.L. Campos, Advances in colloidal processing of rare earth particles, *Current Smart Mater.* (2017).
- [27] M. Marina, M.Z.M. Zamzuri, M.N. Derman, M.A. Selamat, Z. Nooraizedfiza, Comparison study in consolidation of yttria reinforced iron-chromium composites using conventional and microwave sintering technique, *Adv. Mater. Eng. Technol.* II 594–595 (2014) 832–836.
- [28] F. Hayashi, M. Tanaka, D.M. Lin, M. Iwamoto, Surface structure of yttrium-modified ceria catalysts and reaction pathways from ethanol to propene, *J. Catal.* 316 (2014) 112–120.
- [29] X.M. Han, X. Feng, X.W. Qi, X.Q. Wang, M.Y. Li, The photoluminescent properties of Y2O3:Bi3+, Eu3+, Dy3+ phosphors for white-light-emitting diodes, *J. Nanosci. Nanotechnol.* 14 (2014) 3387–3390.
- [30] A. Jyotsana, G.S. Maurya, A.K. Srivastava, A.K. Rai, B.K. Ghosh, Synthesis and electrical properties of Y2O3: Dy3+ & Eu3+ nanoparticles, *Appl. Phys. A-Mater.* 117 (2014) 1269–1274.
- [31] T. Mongstad, A. Thøgersen, A. Subrahmanyam, S. Karazhanov, The electronic state of thin films of yttrium, yttrium hydrides and yttrium oxide, *Sol. Energy Mater. Sol. C* 128 (2014) 270–274.
- [32] M.A. Auger, V. de Castro, T. Leguey, J. Tarcisio-Costa, M.A. Monge, A. Munoz, R. Pareja, Effect of yttrium addition on the microstructure and mechanical properties of ODS RAF steels, *J. Nucl. Mater.* 455 (2014) 600–604.
- [33] J. Hostasa, J. Matejicek, B. Nait-Ali, D.S. Smith, W. Pabst, L. Esposito, Thermal properties of transparent Yb-Doped YAG ceramics at elevated temperatures, *J. Am. Ceram. Soc.* 97 (2014) 2602–2606.
- [34] M.A. Yar, S. Wahlberg, M.O. Abuelnaga, M. Johnsson, M. Muhammed, Processing and sintering of yttrium-doped tungsten oxide nanopowders to tungsten-based composites, *J. Mater. Sci.* 49 (2014) 5703–5713.
- [35] X.B. Li, Q.Q. Zhang, S.Y. Ma, G.X. Wan, F.M. Li, X.L. Xu, Microstructure optimization and gas sensing improvement of ZnO spherical structure through yttrium doping, *Sensor. Actuator. B Chem.* 195 (2014) 526–533.
- [36] F.B. Vetrone, J.-C. Capobianco, J. A. Luminescence, Optical Spectroscopy and Applications of Rare Earth Doped Y2O3 Nanocrystals., American Scientific Publishers, Stevenson Ranch, CA, 2003.
- [37] L. Zhang, D.Y. Jiang, J.F. Xia, C.X. Li, N. Zhang, Q. Li, Novel luminescent yttrium oxide nanosheets doped with Eu3+ and Tb3+, *RSC Adv.* 4 (2014) 17648–17652.
- [38] S.C. Santos, O. Rodrigues, L.L. Campos, Bio-prototyping of europium-yttria based rods for radiation dosimetry, *Mater. Chem. Phys.* 199 (2017) 557–566.
- [39] Y.N. Xu, Z.Q. Gu, W.Y. Ching, Electronic, structural, and optical properties of crystalline yttria, *Phys. Rev. B* 56 (1997) 14993–15000.
- [40] A. Gajović, N. Tomasić, I. Djerdj, D.S. Su, K. Furić, Influence of mechanochanical processing to luminescence properties in Y2O3 powder, *J. Alloys Compd.* 456 (2008) 313–319.
- [41] M. Klintenberg, S. Edvardsson, J.O. Thomas, Energy level and oscillator strength calculations for Er3+:Y2O3: a molecular dynamics based study, *J. Alloys Compd.* 275–277 (1998) 174–176.
- [42] H.R. Hoekstra, K.A. Gingerich, High-pressure B-Type polymorphs of some rare-earth sesquioxides, *Science* 146 (1964), 1163–&.
- [43] V. Gourlaouen, G. Schneedecker, A.M. Lejus, M. Boncoeur, R. Collongues, Metastable phases in yttrium-oxide plasma spray deposits and their effect on coating properties, *Mater. Res. Bull.* 28 (1993) 415–425.
- [44] A. Navrotsky, L. Benoit, H. Lefebvre, Direct calorimetric measurement of enthalpies of phase transitions at 2000 degrees-2400 degrees C in yttria and zirconia, *J. Am. Ceram. Soc.* 88 (2005) 2942–2944.
- [45] X. Qin, Y.G. Ju, S. Bernhard, N. Yao, Flame synthesis of Y2O3 : Eu nanoparticles using ethanol as precursor solvents, *J. Mater. Res.* 20 (2005) 2960–2968.
- [46] E.R. Andrievskaya, Phase equilibria in the refractory oxide systems of zirconia, hafnia and yttria with rare-earth oxides, *J. Eur. Ceram. Soc.* 28 (2008) 2363–2388.

- [47] G. Schaack, J.A. Koningstein, Phonon and electronic Raman spectra of cubic rare-earth oxides and isomorphous yttrium oxide, *J. Opt. Soc. Am.* 60 (1970) 1110–1115.
- [48] J.H. Lunsford, Esr of adsorbed oxygen species, *Catal. Rev.* 8 (1973) 135–157.
- [49] E. Wuilloud, B. Delley, W.D. Schneider, Y. Baer, Spectroscopic evidence for localized and extended F-Symmetry states in CeO<sub>2</sub>, *Phys. Rev. Lett.* 53 (1984) 202–205.
- [50] A. Pfau, K.D. Schierbaum, The electronic-structure of stoichiometric and reduced CeO<sub>2</sub> surfaces - an xps, ups and Heeels study, *Surf. Sci.* 321 (1994) 71–80.
- [51] H. Norenberg, G.A.D. Briggs, Defect structure of nonstoichiometric CeO<sub>2</sub>(111) surfaces studied by scanning tunneling microscopy, *Phys. Rev. Lett.* 79 (1997) 4222–4225.
- [52] D.R. Mullins, S.H. Overbury, D.R. Huntley, Electron spectroscopy of single crystal and polycrystalline cerium oxide surfaces, *Surf. Sci.* 409 (1998) 307–319.
- [53] M.A. Henderson, C.L. Perkins, M.H. Engelhard, S. Thevuthasan, C.H.F. Peden, Redox properties of water on the oxidized and reduced surfaces of CeO<sub>2</sub>(111), *Surf. Sci.* 526 (2003) 1–18.
- [54] M.A. Panhans, R.N. Blumenthal, A thermodynamic and electrical-conductivity study of nonstoichiometric cerium dioxide, *Solid State Ionics* 60 (1993) 279–298.
- [55] Y. Osada, S. Koike, T. Fukushima, S. Ogasawara, T. Shikada, T. Ikariya, Oxidative coupling of methane over Y<sub>2</sub>O<sub>3</sub>-Cao catalysts, *Appl. Catal.* 59 (1990) 59–74.
- [56] V. Singh, V.K. Rai, I. Ledoux-Rak, S. Watanabe, T.K.G. Rao, J.F.D. Chubaci, L. Badie, F. Pelle, S. Ivanova, NIR to visible up-conversion, infrared luminescence, thermoluminescence and defect centres in Y(2)O(3) : Er phosphor, *J. Phys. D Appl. Phys.* 42 (2009).
- [57] O.M. Bordun, Influence of oxygen vacancies on the luminescence spectra of Y<sub>2</sub>O<sub>3</sub> thin films, *J. Appl. Spectrosc.* 69 (2002) 430–433.
- [58] J.M. Costantini, F. Beuneu, D. Gourier, C. Trautmann, G. Calas, M. Toulemonde, Colour centre production in yttria-stabilized zirconia by swift charged particle irradiations, *J. Phys. Condens. Matter* 16 (2004) 3957–3971.
- [59] C.A. Hutchison, The magnetic susceptibility of beo, *Phys. Rev.* 75 (1949) 465–466.